

Roberto Palma, José L. Pérez-Aparicio, and Pedro Museros

Finite element modeling of energy harvesters: application to vibrational devices

Abstract: This chapter presents the set of governing equations to study the behavior of active materials that have an intrinsic ability for coupling several branches of physics and, consequently, are commonly used for manufacturing harvesters. Once the equations are defined, a numerical formulation based on the finite element method is developed in order to model these materials. In particular, this chapter studies the energy production from the mechanical vibrations present in high-speed railway bridges. For this purpose, a review of the basic parameters of these bridges, their vibrations, frequencies and the dynamic characteristics are highlighted. Then, cantilever harvesters made out of piezoelectric and piezomagnetic materials are simulated under typical mechanical vibrations, and several conclusions are highlighted.

Keywords: Active materials, finite element method, piezoelectric devices, piezomagnetic devices, high-speed bridges, vibrating harvesters

1 Introduction

As is well known, the energy obtained from residual sources is called renewable or clean energy. Depending on the level of power produced, this renewable energy is commonly divided into two groups:

- Macro-energy harvesting plants, generating in the order of [kW] or [MW], for example: watermill, geothermal and solar energies. These plants are designed as alternatives to traditional fossil-fuel-based and nuclear plants.
- Micro-energy harvesting technologies, which produce in the order [mW] or [μ W], and are based on residual sources such as mechanical vibrations, heat, sunlight, chemical or biological sources, etc. In contrast to macro-energy, this technology is conceived as an alternative to conventional electro-chemical batteries.

The present chapter is focused on micro-energy technology using harvesters. In general, harvesters are manufactured with modern materials, denominated active or smart materials that have the intrinsic ability to couple up to four physic energies, such as mechanical, thermal and electromagnetism. According to [1], the global market for smart materials was 26 USD billion in 2014 and will be approximately 42 USD billion in 2019.

Roberto Palma, Department of Mechanical Engineering and Construction, Universitat Jaume I, Spain
José L. Pérez-Aparicio, **Pedro Museros**, Department of Continuum Mechanics and Theory of Structures, Universitat Politècnica de València, Spain

There are many examples of energy harvesting applications depending on the residual sources. For instance, thermoelectric devices are used to generate energy from residual heat and piezoelectric/piezomagnetic materials from residual mechanical vibrations.

In connection with thermoelectric materials, they are commonly used to reduce the weight in aeronautics and astronautics. In particular, the radioisotope thermoelectric generator (RTG) is an electrical generator that draws its energy from the heat released by radioactive disintegration of the fuel – usually plutonium. The assembly of an RTG can be seen in Figure 1, consisting of a container of nuclear fuel that generates the necessary heat through a nuclear fission. This heat is converted into electrical energy by thermocouples in the radioisotope heat unit, powered by a thermal flux between the core at up to 1200 [K] and the hot spot, usually a liquid metal cooling system connected to the space at up to 300 [K]. In spite of this very large temperature increment, the efficiency usually lies between 4–7%, with a maximum of 10%.

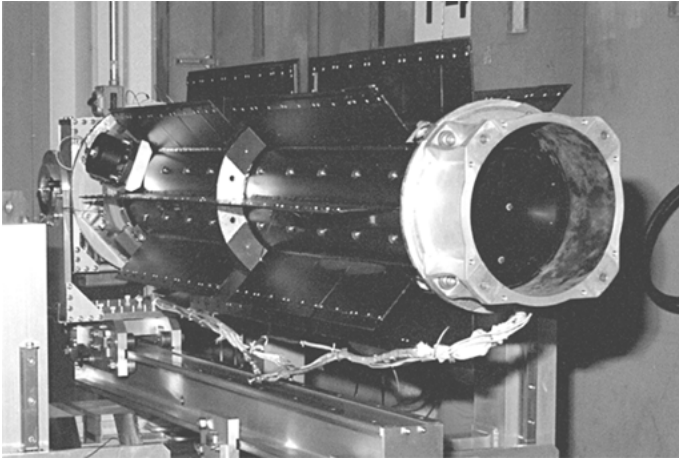


Fig. 1: Radioisotope thermoelectric generator for space rover, [2].

Concerning vibrating harvesters, they are used for wearing shoes and backpacks, for computer hard disks, for medical micro-robots and, especially, for energy recovering from environmental vibrations, see [3]. In this context, the possibility of energy harvesting from vibrations of bridges is a very new field. Recently, [4] and others have been investigating the feasibility of recovering electric energy for high-speed trains passing over a bridge. Small amounts of electric energy can be recovered by the induced vibrations, and this energy be used for the WiFi signals of structural health monitoring (SHM) systems.

In short, the energy generation from residual sources – such as heating and mechanical vibrations – is a challenge for both engineering and scientific communities.

Therefore, both the theoretical understanding and numerical modeling are important challenges in order to design sophisticated harvesters that generate as much energy as possible. From a modeling point of view, some of the authors of the present chapter have published several numerical formulations based on the finite element (FE) method to study active materials, see [5] to [6].

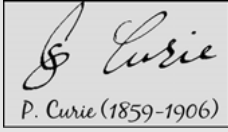
From a practical point of view, it is also very important to know the energy orders of magnitude that the residual sources can yield, for instance, temperature gradients in buildings, mechanical vibration amplitudes in bridges, etc. In this way, one author of the present chapter has wide experience in the design of high-speed railway bridges, see [7] to [8].

On these grounds, this chapter defines the active materials and their advantages in comparison with classical materials, see Section 2. Then, an outline of the governing equations that theoretically describe the behavior of active materials is reported in Section 3. In particular, the main equations of continuum mechanics, electromagnetism and thermodynamics, are briefly described. Section 4 introduces the FE formulation to numerically model the active materials. First, for the sake of clarity, a brief outline of the FE method is introduced. Regarding practical applications, Section 5 presents a summary of railway bridges and their mechanical vibrations produced by passing vehicles. Finally, numerical simulations of harvesters that produce energy from mechanical vibrations are reported. In particular, basic cantilever beams made of both piezoelectric and piezomagnetic materials are simulated, and a comparison between both is highlighted.

Through the chapter, several simplifications are introduced. From a mechanical point of view, small strain is considered: it is a good approximation for most of the harvester applications, since classical active materials are made out of ceramics. Electrodynamically, free electromagnetic sources such as free electric charges and currents are not considered, since these active materials are, in general, non-conductors. Furthermore, the high frequencies produced by the electromagnetic field (speed of light) are neglected in comparison with the mechanical frequencies; this is a reasonable approximation, since this chapter deals with the energy production from the residual mechanical vibrations. Finally, and from a thermodynamical point of view, conservative materials are considered, namely, dissipations generated by the heating of harvesters are neglected.

2 Active materials

In classical physics, every cause has an effect. For instance, applying forces to an elastic body (cause) produces strains (effect); applying electric fields to a dielectric medium (cause) polarizes the material (effect), etc.

Historical note

P. Curie (1859-1906)

Early work on active materials was carried out by the French brothers Jacques and Pierre Curie; in particular, piezoelectricity was discovered in 1880 by both. Jacques Curie (1855–1941) was Professor of Mineralogy at the Université de Montpellier. His younger brother Pierre Curie (1859–1906) received the Nobel Prize in Physics with his wife, Marie Curie, and Henri Becquerel. Signature taken from *Wikipedia*.

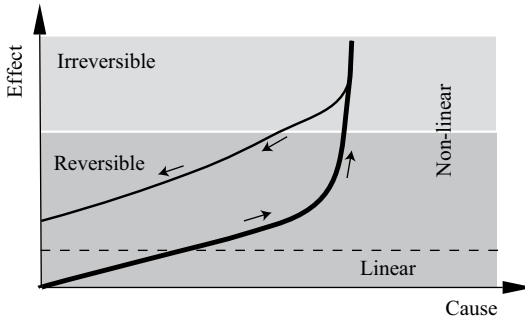


Fig. 2: Cause-effect curve. Two regions are observed: linear/non-linear and reversible/irreversible.

Causes and effects are related by constitutive equations that describe the behavior of the material and are obtained by experimental techniques. For example, in mechanics, the stress-strain curve is calculated by applying equal and opposite forces at the ends of a bar and measuring its relative deformation. From this curve, several important material properties, such as the modulus of elasticity and ductility, are obtained. Figure 2 shows a general cause-effect curve in which two regions are observed:

- Linear and non-linear. The linear region is mathematically represented by first-order material properties in a Taylor series expansion. On the contrary, the non-linear region requires high-order material properties that, in general, depend on the high-order expressions of the causes and/or effects.
- Reversible and irreversible regions. The former represents a hypothetical behavior for which the entropy of the system is conserved. For this reason, the material properties inside this region are denominated conservative. In contrast, the irreversible region is characterized by the increasing of the entropy and, consequently, by the production of heat. For example, plasticity is an irreversible response for which the internal structure of the material is irreversibly transformed and heat is dissipated. Therefore, the initial state is not recovered when the cause ceases; this process is path-dependent.

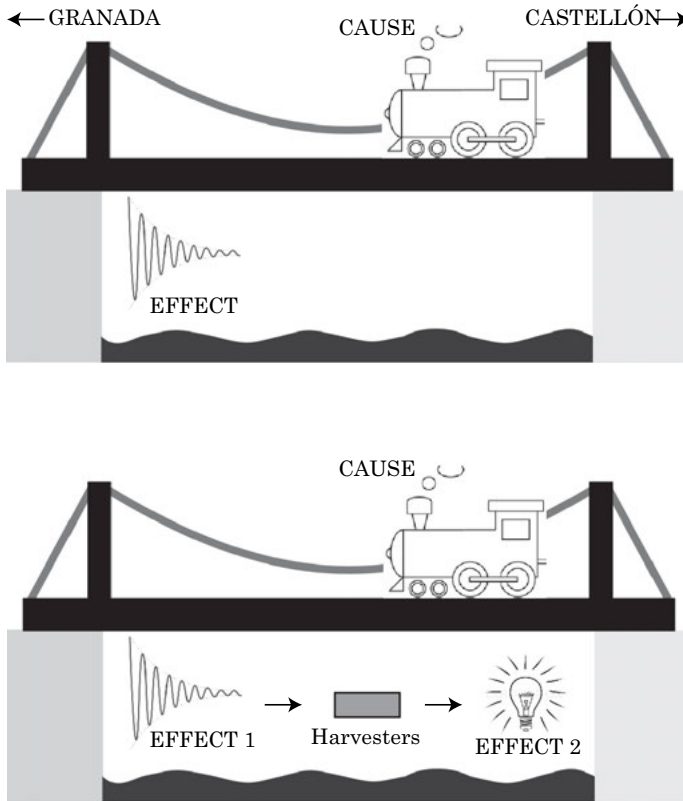


Fig. 3: Passage of a train over a bridge. Top: the train (cause) produces mechanical vibrations (effect). Bottom: the bridge incorporates harvesters made of active materials that produce electrical energy from mechanical vibrations and, consequently, the train generates two effects.

Traditional materials – denominated *passive* materials in the remainder of this chapter –, are characterized by a one-to-one function between cause and effect, namely, stresses generate strains and vice versa. For example, consider a railway bridge made of passive materials such as concrete and steel. The passage of a train over the bridge (cause) generates mechanical vibrations (effect), as observed in Figure 3 (top). On the contrary, active materials are characterized for their intrinsic ability to couple several branches of physics; consequently, a cause produces one or more effects. Continuing with the bridge example, consider that this bridge also incorporates harvesters made out of active materials. Now, the mechanical vibrations generate electrical energy, see Figure 3 (bottom). Therefore, the passage of a train generates two sequential effects: mechanical vibrations and electrical energy.

As commented, in this work, an active material can couple up to four fields: thermal, mechanical, electrical and magnetic. Heckmann's diagram [9] allows us

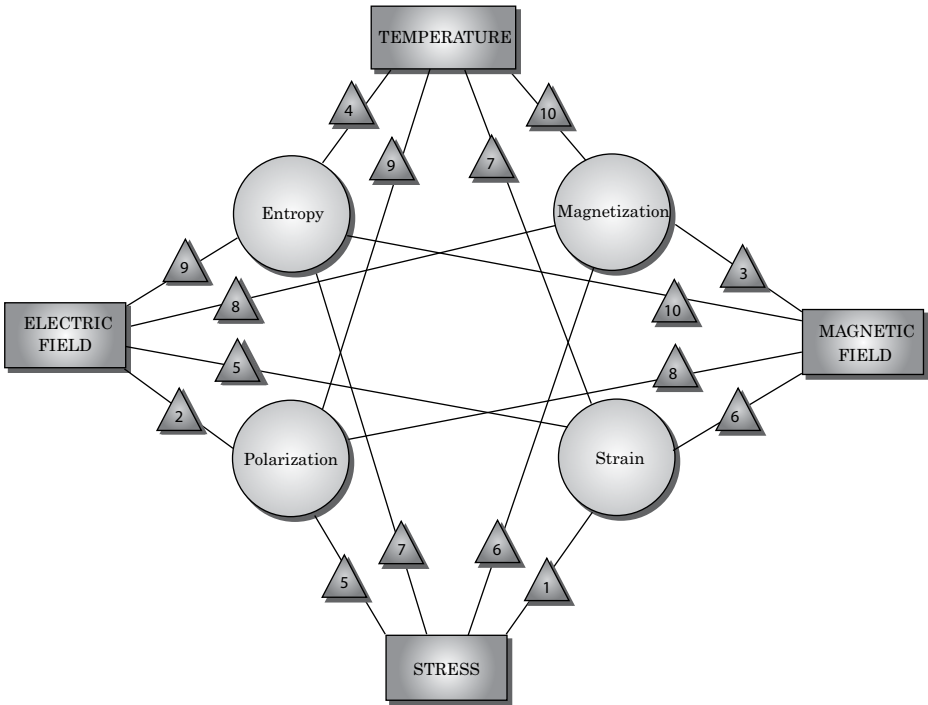








Fig. 4: Heckmann’s diagram: causes, effects and first-order properties represented by rectangles, circles and triangles, respectively. Material properties are clarified in Tables 1, 2; picture taken from [9].

to schematically visualize these couplings, as shown in Figure 4. The causes are represented by rectangles and the effects by circles. Then, the first-order materials properties that relate causes and effects are represented by triangles, and they are listed in Tables 1 and 2. Table 1 refers to the main interactions, namely, the *passive* properties; Table 2 shows the coupling, the *active* properties.

Tab. 1: First-order *passive* properties. Triangles in first column refer to Figure 4. Table taken from [9].

Symbol	Conjugate variables	Passive property
△ 1	Stress – Strain	Elastic tensor
△ 2	Electric field – Polarization	Electric susceptibility
△ 3	Magnetic field – Magnetization	Magnetic susceptibility
△ 4	Temperature – Entropy	Heat capacity

Tab. 2: First-order *active* properties. Triangles in first column refer to Figure 4. Table taken from [9].

Symbol	Conjugate variables	Active property
	Mechanic – Electric	Direct, converse piezoelectric
	Mechanic – Magnetic	Direct, converse piezomagnetic
	Mechanic – Thermal	Thermal expansion, piezocaloric
	Electric – Magnetic	Direct, converse magnetoelectric
	Electric – Thermal	Direct, converse pyroelectric
	Magnetic – Thermal	Direct, converse pyromagnetic

In short, the active materials allow the production of energy from residual sources such as heat, mechanical vibrations, etc. These materials will be studied in the remainder of this chapter. Furthermore, since these materials couple several fields of physics, the following section introduces the basic governing equations of continuum physics.

3 Continuum physics

Consider a continuum solid of domain Ω , boundary Γ and its outward normal \mathbf{n} . This solid is subjected to mechanical, electromagnetism and thermal energies and, consequently, the governing equations of the four fields must be considered.

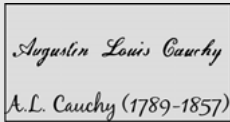
For the sake of convenience, the present chapter uses both tensor and matrix notations. For the first, the following tensor operators are used:

- Scalar product or single contraction denoted by the symbol (\cdot) : $\mathbf{a} \cdot \mathbf{b} = a_i b_i$.
- Double contraction denoted by the symbol $(:)$: $\mathbf{A} : \mathbf{B} = A_{ij} B_{ij}$.
- Dyadic or outer product denoted by the symbol (\otimes) : $(\mathbf{a} \otimes \mathbf{b})_{ij} = a_i b_j$.
- Cross product denoted by the symbol (\times) : $(\mathbf{a} \times \mathbf{b})_i = \epsilon_{ijk} a_j b_k$, where ϵ is the Levi-Civita tensor.
- The transposition is denoted by $()^\top$.
- The symbol ∇ denotes the *Del* operator.

3.1 Outline of continuum mechanics

Classical continuum mechanics is a branch of continuum physics that studies the kinematics and the mechanical response of deformable bodies subjected to the action of forces. Firstly, the word deformable refers to the capacity to change the medium shape – conversely to the rigid body mechanics that studies non-deformable solids. Secondly, the term continuum indicates that matter completely fills the medium, that is, the medium is assumed to be continuous. This assumption is known as the continuum hypothesis [9]. Finally, and considering this hypothesis, each point of the body (commonly called material point) can be identified by a position vector and, consequently, the tensor algebra can be applied to study the motion and deformation of solids.

Historical note



Augustin Louis Cauchy
A.L. Cauchy (1789-1857)

The French mathematician Augustin Louis Cauchy (1789–1857) pioneered the use of continuum instead of discrete models. In spite of his initial 3 years of working as an engineer, he was more attracted to the abstract beauty of mathematics. Cauchy was a prolific scientist: in continuum mechanics he holds 16 theorems. Signature taken from *Wikipedia*.

3.1.1 Kinematics

Consider a continuum body before (at time $t = 0$) and after deformation (at time t ; Figure 5). The position of a material point P_0 inside a domain Ω_0 with border Γ_0 “before”

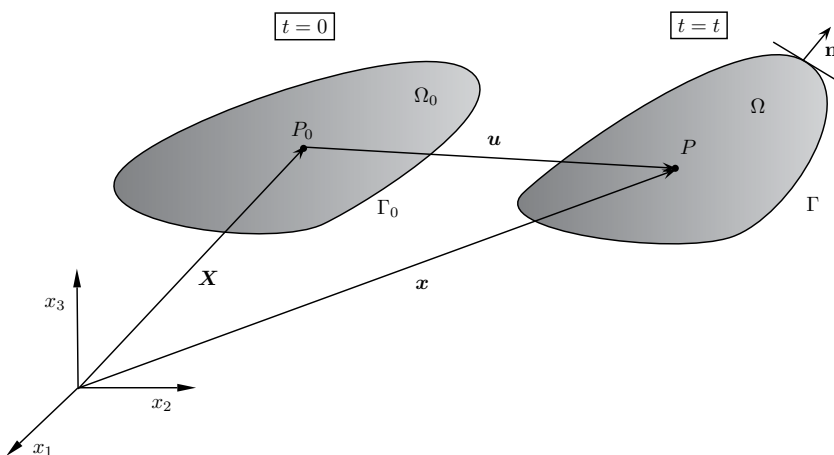


Fig. 5: Continuum body before and after deformation.

is located by \mathbf{X} ; “after” the point becomes P inside another domain Ω of boundary Γ and located by \mathbf{x} . From vector calculus, the displacement \mathbf{u} of any material point can be represented by:

$$\mathbf{u}(\mathbf{X}, t) = \mathbf{x}(\mathbf{X}, t) - \mathbf{X}(t) . \quad (1)$$

The dependency of \mathbf{u} and \mathbf{x} on \mathbf{X} is commonly denominated as “Lagrange coordinates” in the continuum mechanics community. However, under the assumption of small displacements $\mathbf{X} \approx \mathbf{x}$, the notation $\mathbf{u}(\mathbf{x}, t)$ is adopted in the remainder of the present work.

3.1.2 Strain measure

An objective strain measure can be defined as the change of length and rotation of an elementary differential of displacement. Mathematically, this definition can be expressed as:

$$d\mathbf{u}(\mathbf{x}, t) = \frac{\partial \mathbf{u}}{\partial \mathbf{x}} \cdot d\mathbf{x} = \mathbf{u} \otimes \nabla \cdot d\mathbf{x} , \quad (2)$$

where the non-symmetric tensor $\mathbf{u} \otimes \nabla$ is called the displacement gradient. As commented, this tensor contains information on the change of lengths and on the rotations of $d\mathbf{u}$. In particular, it is observed in Figure 6 that the information relative to the change of lengths is stored in the symmetric part of $(\mathbf{u} \otimes \nabla)^{sy}$ and the rotation in the skew-symmetric $(\mathbf{u} \otimes \nabla)^{sk}$.

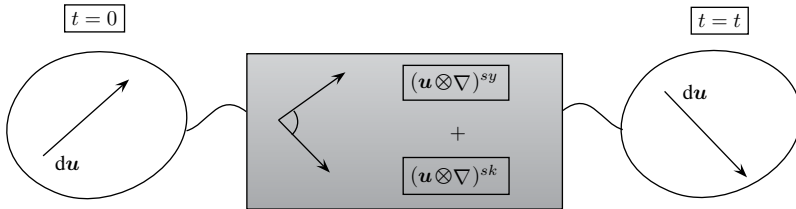


Fig. 6: Box representing the deformation process: elongation $(\mathbf{u} \otimes \nabla)^{sy}$ and rotation $(\mathbf{u} \otimes \nabla)^{sk}$.

According to the theory of tensor algebra, any tensor can be decomposed in symmetric and skew-symmetric parts. Therefore, the displacement gradient can be expressed as:

$$\mathbf{u} \otimes \nabla = \frac{1}{2}(\mathbf{u} \otimes \nabla + \nabla \otimes \mathbf{u}) + \frac{1}{2}(\mathbf{u} \otimes \nabla - \nabla \otimes \mathbf{u}) , \quad (3)$$

Since the rotations do not produce deformation, the strain measure is given by the symmetric part of (3); under the assumption of small strains, the symmetric displacement gradient is finally given by:

$$\mathbf{S} = \frac{1}{2}(\mathbf{u} \otimes \nabla + \nabla \otimes \mathbf{u}) = \nabla^{sy} \mathbf{u} , \quad (4)$$

where the symbol ∇^{sy} is used for simplicity and \mathbf{S} denotes the second-order small strain tensor.

For the sake of convenience, \mathbf{S} is expressed in Voigt's notation with indexes 11 = 1, 22 = 2, 33 = 3, 12 = 4, 23 = 5, 13 = 6 to obtain:

$$\{\mathbf{S}\} = \{S_1, S_2, S_3, S_4, S_5, S_6\}^T \quad (5)$$

As observed, Voigt's notation allows us to represent a symmetric second-order tensor by a vector of six coefficients.

3.1.3 Linear momentum balance

From the second Newton's law, the linear momentum balance states that the rate of momentum $\mathbf{p} = \rho_m \dot{\mathbf{u}}$ is equal to the total forces acting on the body of Figure 7 (ρ_m is the mass density). Notice that the domain is drawn after deformation, commonly denominated current configuration.

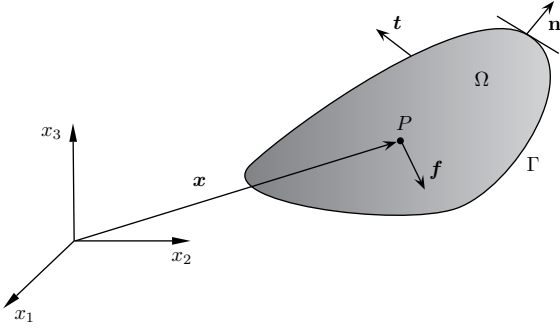


Fig. 7: Forces acting on continuum body after deformation.

The forces acting on Ω can be classified into long-range \mathbf{f} and short-range \mathbf{t} forces. The former represents the forces exerted by external fields such as gravity, and the latter the forces that interact among material points.

On this basis, the linear momentum balance is mathematically stated as:

$$\frac{d}{dt} \int_{\Omega} \mathbf{p} \, d\Omega = \int_{\Gamma} \mathbf{t} \, d\Gamma + \int_{\Omega} \mathbf{f} \, d\Omega . \quad (6)$$

Considering the notation \mathbf{T}^c as the second-order Cauchy stress tensor, the mass conservation $d\rho_m/dt = 0$, Cauchy's lemma $\mathbf{t} = (\mathbf{T}^c)^T \cdot \mathbf{n}$ and applying the divergence theorem to the first term on the right-hand side (6), the linear momentum balance in local form becomes:

$$\rho_m \dot{\mathbf{u}} = \nabla \cdot (\mathbf{T}^c)^T + \mathbf{f} . \quad (7)$$

3.1.4 Angular momentum balance

The angular momentum balance states that in any inertial frame the rate of change of the torque is equal to the total momentum generated by the forces acting on the body. Considering the Figure 7 and (6), this equality is mathematically expressed as:

$$\frac{d}{dt} \int_{\Omega} \mathbf{x} \times \mathbf{p} \, d\Omega = \int_{\Gamma} \mathbf{x} \times \mathbf{t} \, d\Gamma + \int_{\Omega} \mathbf{x} \times \mathbf{f} \, d\Omega. \quad (8)$$

Again, taking into account mass conservation, Cauchy's lemma, the divergence theorem to the first term of (8) on the right-hand side and using (6), the angular momentum balance reads:

$$\boldsymbol{\epsilon} : \mathbf{T}^c = \mathbf{0} \quad \Rightarrow \quad \mathbf{T}^c = (\mathbf{T}^c)^T. \quad (9)$$

In conclusion, the symmetry of the Cauchy stress automatically guarantees the balance of angular momentum. As for \mathbf{S} , \mathbf{T}^c , it can be expressed in Voigt's notation as:

$$\{\mathbf{T}^c\} = \{T_1^c, T_2^c, T_3^c, T_4^c, T_5^c, T_6^c\}^T. \quad (10)$$

3.2 Outline of continuum electrodynamics

Classical electrodynamics (also called classic electromagnetism) is a branch of continuum physics that deals with the interactions between matter and electric charges and currents. This formalism is founded on the Maxwell's equations and on the Lorentz force.

Historical note



Although many scientists worked on electromagnetism, the Scottish mathematician James Clerk Maxwell (1831–1879) achieved the formulation of the classical theory of electromagnetism, denominated “second great unification in physics” after the first was realized by Isaac Newton. Signature taken from *Wikipedia*.

3.2.1 Maxwell equations

Maxwell's equations are a set of four coupled and empirical equations that relate the macroscopic variables of electromagnetism: electric field \mathbf{E} , electric displacement \mathbf{D} , magnetic field \mathbf{H} and magnetic induction \mathbf{B} . Furthermore, the sources of electromag-

netism, free electric charges ρ_q^f and free electric currents \mathbf{j}^f also appear in Maxwell's equations:

$$\begin{aligned}\nabla \cdot \mathbf{D} &= \rho_q^f, \\ \nabla \cdot \mathbf{B} &= 0, \\ \nabla \times \mathbf{E} + \frac{\partial \mathbf{B}}{\partial t} &= \mathbf{0}, \\ \nabla \times \mathbf{H} - \frac{\partial \mathbf{D}}{\partial t} - \mathbf{j}^f &= \mathbf{0}.\end{aligned}\tag{11}$$

The first equation is denominated electric Gauss' law and states that the scalar sources of the electric field are the free electric charges. The second is called magnetic Gauss' law and establishes the absence of magnetic monopoles in nature, namely, the magnetic field is solenoidal. The third law is the Maxwell–Faraday law and states that the rate of change of a magnetic field generates an electric field. Therefore, this law couples both electric and magnetic fields. Finally, the fourth equation is Ampère's law, which asserts that the free electric currents and the rate of change of the electric displacement produce magnetic fields. Consequently, this law also couples both fields.

3.2.2 Electromagnetic potentials

In accordance with the Helmholtz theorem – also known as the fundamental theorem of vector calculus [9] – and according to Maxwell's laws of (11), there are four electromagnetic potentials:

- Two scalar potentials obtained from the Maxwell–Faraday and Ampère laws.
- Two vector potentials deduced from the electric and magnetic Gauss' laws.

Nevertheless, in the present chapter, the free sources ρ_q^f and \mathbf{j}^f and the partial derivatives $\partial \mathbf{B} / \partial t$ and $\partial \mathbf{D} / \partial t$ are assumed to be zero. This is a good and reasonable approximation for most applications of harvesters, since they are constructed with polarizable/magnetizable media and the frequencies of the mechanical vibrations are several orders of magnitude lower than the electromagnetic ones.

Assuming $\rho_q^f = 0$, $\mathbf{j}^f = \mathbf{0}$, the electric V and magnetic φ scalar potentials can be obtained from the Maxwell–Faraday and Ampère laws, respectively [9]:

$$\begin{aligned}\nabla \times \mathbf{E} = \mathbf{0} &\quad \Rightarrow \quad \mathbf{E} = -\nabla V, \\ \nabla \times \mathbf{H} = \mathbf{0} &\quad \Rightarrow \quad \mathbf{H} = -\nabla \varphi.\end{aligned}\tag{12}$$

Furthermore, these scalar potentials are more amenable for an FE formulation, as was reported in [9]. Finally and for convenience, the electromagnetic constitutive equations that relate polarization \mathbf{P} and magnetization \mathbf{M} vectors with \mathbf{E} , \mathbf{D} and \mathbf{H} , \mathbf{B} , re-

spectively, are introduced in the same reference:

$$\begin{aligned} \mathbf{D} &= \mathbf{P} + \epsilon_0 \mathbf{E}, \\ \mathbf{B} &= \mu_0 (\mathbf{H} + \mathbf{M}). \end{aligned} \quad (13)$$

3.2.3 Linear momentum balance

The linear momentum balance of electromagnetism is obtained by combining Maxwell's laws and Lorentz forces. There exist four representations of the electromagnetic linear momentum, see [9], closely related to the choice of the Poynting vector. Despite the fact that the best choice of this vector has generated controversy in the literature (for instance, the famous Abraham–Minkowski debate), in the present chapter, the Minkowski representation is assumed. Taking into account this representation, the linear momentum balance in local form is given by [10]:

$$\frac{\partial}{\partial t} (\mathbf{D} \times \mathbf{B}) = \nabla \cdot (\mathbf{T}^{\text{EM}})^{\text{T}} - \mathbf{f}^{\text{EM}}, \quad (14)$$

where \mathbf{T}^{EM} and \mathbf{f}^{EM} denote the Maxwell stress tensor and the Lorentz forces, respectively. Obviously, both terms depend on the electromagnetic variables and, in the absence of free sources, are given by:

$$\begin{aligned} \mathbf{T}^{\text{EM}} &= \mathbf{D} \otimes \mathbf{E} + \mathbf{B} \otimes \mathbf{H} - \frac{1}{2} (\mathbf{D} \cdot \mathbf{E} + \mathbf{B} \cdot \mathbf{H}) \mathbf{I}, \\ \mathbf{f}^{\text{EM}} &= \frac{1}{2} (\nabla \otimes \mathbf{E} \cdot \mathbf{D} - \nabla \otimes \mathbf{D} \cdot \mathbf{E} + \nabla \otimes \mathbf{H} \cdot \mathbf{B} - \nabla \otimes \mathbf{B} \cdot \mathbf{H}). \end{aligned} \quad (15)$$

3.2.4 Angular momentum balance

As deduced in (9), the mechanical angular momentum balance is guaranteed by the symmetry of the Cauchy stress tensor. Similarly, the electromagnetic angular momentum balance requires the symmetry of \mathbf{T}^{EM} .

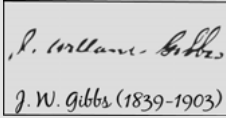
In vacuum (absence of matter), \mathbf{T}^{EM} is symmetric; however, its symmetry in ponderable media (media with matter) has generated controversy in the literature [9]. Under classical continuum physics, the definition of a total stress tensor composed of two non-symmetric tensors (Cauchy and Maxwell) is the best approach.

The use of a total stress implies the modification of the classical traction vector \mathbf{t} (Figure 7), by the mechatronic vector \mathbf{t}_{EM} , which contains information of both mechanic and electromagnetic fields. For more details on the non-symmetry of the Maxwell tensor, see the recently published scientific article by the present authors [6].

3.3 Outline of thermodynamics

Thermodynamics is a branch of continuum physics that deals with the conservation and conversion of the energy, among several fields such as mechanical, thermal, electromagnetic fields, etc. Therefore, this formalism is the cornerstone to theoretically study harvesters.

Historical note



The American scientist Josiah Willard Gibbs (1839–1903) introduced the idea of incorporating the entropy into the internal energy of a system. Therefore, he was a pioneer in combining the first and second laws of thermodynamics and, consequently, he is the father of modern thermodynamics. It was declared that “Gibbs’s name not only in America but in the whole world will ever be reckoned among the most renowned theoretical physicists of all times”. Signature taken from *Wikipedia*.

The first law of thermodynamics states the conservation of the total energy in a closed system as: the total energy U is equal to the sum of heat Q and work W performed on the system, mathematically:

$$dU = \delta Q + dW, \quad (16)$$

where the symbols $-d-$ and $-\delta-$ denote exact and inexact differentials, respectively. As observed, the heat is an inexact differential since it is path-dependent, namely, part of the total energy is irreversibly converted into heat. An example of an irreversible process is the mechanical plastic deformation for which part of the mechanical energy is employed in the transformation of the internal structure of the material. Then, overheating is produced – heat is dissipated – and the initial state of the material is never recovered.

As commented, this chapter deals with conservative processes for which the effects of the temperature are neglected. Consequently, $\delta Q = 0$ and $dU = dW$.

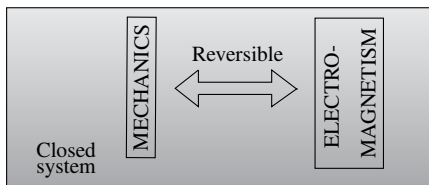


Fig. 8: Reversible exchanges of energies between mechanical and electromagnetic fields with thermal interaction neglected.

Consider the closed thermodynamical system shown in Figure 8. The system is composed of mechanical and electromagnetic energies that can be reversibly exchanged with each other given that $\delta Q = 0$.

As reported in Section 2, causes and effects play an important role in the study of active materials and, consequently, in harvesters. From a thermodynamical point of

view, causes and effects are represented by intensive and extensive variables, respectively, and their products represent the total work performed by the system:

$$dU(\mathbf{S}, \mathbf{P}, \mathbf{M}) = dW(\mathbf{S}, \mathbf{P}, \mathbf{M}) = T^c : d\mathbf{S} + \mathbf{E} \cdot d\mathbf{P} + \mathbf{H} \cdot d\mathbf{M} . \quad (17)$$

Table 3 lists the intensive and extensive variables used in the present work. Simple and double contractions product are used, and the fact that the energy is a scalar variable facilitates the following analyses.

Tab. 3: Intensive (cause) and extensive (effect) variables used in this chapter.

Intensive variables		Extensive variables	
Stress	- T^c	Strain	- \mathbf{S}
Electric field	- \mathbf{E}	Polarization	- \mathbf{P}
Magnetic field	- \mathbf{H}	Magnetization	- \mathbf{M}

There are several thermodynamic potentials to represent the total internal energy of the system. In this work, and for an amenable numerical implementation, it is convenient to use the electromagnetic enthalpy Π , which results from a Legendre transformation of (17) to exchange the pair \mathbf{P}, \mathbf{M} by the corresponding \mathbf{E}, \mathbf{H} :

$$d\Pi(\mathbf{S}, \mathbf{E}, \mathbf{H}) = T^c : d\mathbf{S} - \mathbf{P} \cdot d\mathbf{E} - \mathbf{M} \cdot d\mathbf{H} . \quad (18)$$

Since the problem is conservative, Π can be expressed as an exact differential:

$$d\Pi(\mathbf{S}, \mathbf{E}, \mathbf{H}) = \left. \frac{\partial \Pi}{\partial \mathbf{S}} \right|_{\mathbf{E}, \mathbf{H}} : d\mathbf{S} + \left. \frac{\partial \Pi}{\partial \mathbf{E}} \right|_{\mathbf{S}, \mathbf{H}} \cdot d\mathbf{E} + \left. \frac{\partial \Pi}{\partial \mathbf{H}} \right|_{\mathbf{S}, \mathbf{E}} \cdot d\mathbf{H} , \quad (19)$$

Finally, comparing (18) and (19), the constitutive equations can be obtained from Π as:

$$\begin{aligned} T^c &= \left. \frac{\partial \Pi}{\partial \mathbf{S}} \right|_{\mathbf{E}, \mathbf{H}} , \\ \mathbf{P} &= - \left. \frac{\partial \Pi}{\partial \mathbf{E}} \right|_{\mathbf{S}, \mathbf{H}} , \\ \mathbf{M} &= - \left. \frac{\partial \Pi}{\partial \mathbf{H}} \right|_{\mathbf{S}, \mathbf{E}} . \end{aligned} \quad (20)$$

These three expressions can be arranged to obtain a Hessian matrix to describe the behavior of the material:

$$\begin{Bmatrix} dT^c \\ d\mathbf{P} \\ d\mathbf{M} \end{Bmatrix} = \begin{bmatrix} \frac{\partial T^c}{\partial \mathbf{S}} & \frac{\partial T^c}{\partial \mathbf{E}} & \frac{\partial T^c}{\partial \mathbf{H}} \\ \frac{\partial \mathbf{P}}{\partial \mathbf{S}} & \frac{\partial \mathbf{P}}{\partial \mathbf{E}} & \frac{\partial \mathbf{P}}{\partial \mathbf{H}} \\ \frac{\partial \mathbf{M}}{\partial \mathbf{S}} & \frac{\partial \mathbf{M}}{\partial \mathbf{E}} & \frac{\partial \mathbf{M}}{\partial \mathbf{H}} \end{bmatrix} \begin{Bmatrix} d\mathbf{S} \\ d\mathbf{E} \\ d\mathbf{H} \end{Bmatrix} . \quad (21)$$

In order to obtain the constitutive equations and considering (20), an explicit form of the potential Π must be calculated. In a first and reasonable approximation, this potential can be found by a Taylor expansion in the vicinity of a natural state $\Pi(\mathbf{S} = \mathbf{E} = \mathbf{H} = \mathbf{0}) = 0$ and by keeping in mind the linearity of the problem, to give:

$$\begin{aligned} \Pi(\mathbf{S}, \mathbf{E}, \mathbf{H}) = & \frac{1}{2} \left(\mathbf{S} : \mathbf{C} : \mathbf{S} - \mathbf{E} \cdot \boldsymbol{\epsilon} \cdot \mathbf{E} - \mathbf{H} \cdot \boldsymbol{\mu} \cdot \mathbf{H} \right) \\ & - \mathbf{e}^V : \mathbf{S} \cdot \mathbf{E} - \mathbf{e}^\varphi : \mathbf{S} \cdot \mathbf{H} - \mathbf{H} \cdot \mathbf{v} \cdot \mathbf{E}, \end{aligned} \quad (22)$$

where \mathbf{C} , $\boldsymbol{\epsilon}$, $\boldsymbol{\mu}$, \mathbf{v} , \mathbf{e}^V and \mathbf{e}^φ denote elastic, permittivity, permeability, electromagnetic, piezoelectric and piezomagnetic material tensors, respectively. Finally, considering (13), (22) and (20), the Hessian (21) becomes:

$$\begin{Bmatrix} \mathbf{T}^c \\ \mathbf{D} \\ \mathbf{B} \end{Bmatrix} = \begin{bmatrix} \mathbf{C} & -\mathbf{e}^V & -\mathbf{e}^\varphi \\ \mathbf{e}^V & \boldsymbol{\epsilon} & \mathbf{v} \\ \mathbf{e}^\varphi & \mathbf{v} & \boldsymbol{\mu} \end{bmatrix} \begin{Bmatrix} \mathbf{S} \\ \mathbf{E} \\ \mathbf{H} \end{Bmatrix}. \quad (23)$$

3.4 Summary of governing equations

This section summarizes the governing equations to model conservative active materials under small strains and displacements, for low electromagnetic frequencies and assuming material linearity. The equations are equilibrium and constitutive complemented by the boundary conditions.

3.4.1 Equilibrium equations

For an amenable FE implementation and considering \mathbf{T}^{EM} , the equilibrium equations are the linear momentum balance (7) and the electric and magnetic Gauss laws (11):

$$\begin{aligned} \rho_m \ddot{\mathbf{u}} &= \nabla \cdot \mathbf{T}^T + \mathbf{f}, \\ \nabla \cdot \mathbf{D} &= 0, \\ \nabla \cdot \mathbf{B} &= 0, \end{aligned} \quad (24)$$

where $\mathbf{T}^T = \mathbf{T}^c + (\mathbf{T}^{EM})^{SY}$ is the total stress tensor, composed of both symmetric Cauchy and Maxwell stress tensors.

3.4.2 Material constitution

For the sake of clarity, the multi-coupled constitutive (23) is expressed in matrix form using Voigt's notation (5) and (10):

Piezoelectrics										
$\left\{ \begin{array}{l} T_1 \\ T_2 \\ T_3 \\ T_4 \\ T_5 \\ T_6 \\ D_1 \\ D_2 \\ D_3 \end{array} \right\} =$	$\left[\begin{array}{cccccccccc} C_{11} & C_{12} & C_{13} & 0 & 0 & 0 & 0 & 0 & 0 & -e_{13}^V \\ C_{12} & C_{11} & C_{13} & 0 & 0 & 0 & 0 & 0 & 0 & -e_{13}^V \\ C_{13} & C_{13} & C_{33} & 0 & 0 & 0 & 0 & 0 & 0 & -e_{33}^V \\ 0 & 0 & 0 & C_{66} & 0 & 0 & 0 & 0 & 0 & 0 \\ 0 & 0 & 0 & 0 & C_{44} & 0 & 0 & -e_{15}^V & 0 & 0 \\ 0 & 0 & 0 & 0 & 0 & C_{44} & -e_{15}^V & 0 & 0 & 0 \\ 0 & 0 & 0 & 0 & 0 & e_{15}^V & \epsilon_{11} & 0 & 0 & 0 \\ 0 & 0 & 0 & 0 & e_{15}^V & 0 & 0 & \epsilon_{11} & 0 & 0 \\ e_{13}^V & e_{13}^V & e_{33}^V & 0 & 0 & 0 & 0 & 0 & 0 & \epsilon_{33} \end{array} \right]$	$\left\{ \begin{array}{l} S_1 \\ S_2 \\ S_3 \\ S_4 \\ S_5 \\ S_6 \\ E_1 \\ E_2 \\ E_3 \end{array} \right\},$								
Piezomagnetics										
$\left\{ \begin{array}{l} T_1 \\ T_2 \\ T_3 \\ T_4 \\ T_5 \\ T_6 \\ B_1 \\ B_2 \\ B_3 \end{array} \right\} =$	$\left[\begin{array}{cccccccccc} C_{11} & C_{12} & C_{13} & 0 & 0 & 0 & 0 & 0 & 0 & -e_{13}^\varphi \\ C_{12} & C_{11} & C_{13} & 0 & 0 & 0 & 0 & 0 & 0 & -e_{13}^\varphi \\ C_{13} & C_{13} & C_{33} & 0 & 0 & 0 & 0 & 0 & 0 & -e_{33}^\varphi \\ 0 & 0 & 0 & C_{66} & 0 & 0 & 0 & 0 & 0 & 0 \\ 0 & 0 & 0 & 0 & C_{44} & 0 & 0 & -e_{15}^\varphi & 0 & 0 \\ 0 & 0 & 0 & 0 & 0 & C_{44} & -e_{15}^\varphi & 0 & 0 & 0 \\ 0 & 0 & 0 & 0 & 0 & e_{15}^\varphi & \epsilon_{11} & 0 & 0 & 0 \\ 0 & 0 & 0 & 0 & e_{15}^\varphi & 0 & 0 & \epsilon_{11} & 0 & 0 \\ e_{13}^\varphi & e_{13}^\varphi & e_{33}^\varphi & 0 & 0 & 0 & 0 & 0 & 0 & \epsilon_{33} \end{array} \right]$	$\left\{ \begin{array}{l} S_1 \\ S_2 \\ S_3 \\ S_4 \\ S_5 \\ S_6 \\ H_1 \\ H_2 \\ H_3 \end{array} \right\}.$								
(25)										

As observed, both constitutive matrices are transversely isotropic, since the present active materials are polarized along the x_3 direction.

3.4.3 Boundary conditions

The set of multi-coupled governing equations is mathematically closed by including the boundary conditions. As is common, these equations are composed of natural and essential boundary conditions; the former are called Neumann and the latter Dirichlet equations. Both are given by:

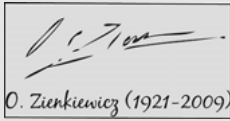
<table style="width: 100%; border: none;"> <tr> <td style="text-align: center; border-bottom: 1px solid black;">Dirichlet type</td> <td style="text-align: center; border-bottom: 1px solid black;">Neumann type</td> <td rowspan="4" style="vertical-align: middle; padding-left: 20px;">(26)</td> </tr> <tr> <td style="text-align: center;">$\mathbf{u} = \bar{\mathbf{u}},$</td> <td style="text-align: center;">$\mathbf{T}^T \cdot \mathbf{n} = \bar{\mathbf{t}}_{EM},$</td> </tr> <tr> <td style="text-align: center;">$V = \bar{V},$</td> <td style="text-align: center;">$\mathbf{D} \cdot \mathbf{n} = \bar{q}_\Gamma,$</td> </tr> <tr> <td style="text-align: center;">$\varphi = \bar{\varphi},$</td> <td style="text-align: center;">$\mathbf{B} \cdot \mathbf{n} = 0,$</td> </tr> </table>	Dirichlet type	Neumann type	(26)	$\mathbf{u} = \bar{\mathbf{u}},$	$\mathbf{T}^T \cdot \mathbf{n} = \bar{\mathbf{t}}_{EM},$	$V = \bar{V},$	$\mathbf{D} \cdot \mathbf{n} = \bar{q}_\Gamma,$	$\varphi = \bar{\varphi},$	$\mathbf{B} \cdot \mathbf{n} = 0,$
Dirichlet type	Neumann type	(26)							
$\mathbf{u} = \bar{\mathbf{u}},$	$\mathbf{T}^T \cdot \mathbf{n} = \bar{\mathbf{t}}_{EM},$								
$V = \bar{V},$	$\mathbf{D} \cdot \mathbf{n} = \bar{q}_\Gamma,$								
$\varphi = \bar{\varphi},$	$\mathbf{B} \cdot \mathbf{n} = 0,$								

where $\bar{\mathbf{u}}, \bar{V}, \bar{\varphi}, \bar{\mathbf{t}}_{EM}$ and \bar{q}_Γ denote prescribed displacements, voltage, scalar magnetic potential, mechatronic vector and electric charges on Γ , respectively.

4 Finite element method

The finite element method (FE) is a numerical technique used to model many problems in science and engineering. Sophisticated situations, such as the governing equations for the active materials reported in Section 3, result in complex systems of partial differential equations for which there are no analytical solutions; but the FE method allows us to approximate these sets of partial differential equations in an algebraic system that can be solved using numerical algorithms. In fact, at present, FE is the more widespread method in technological applications, and a wide number of commercial codes exist. For more details, the reader is referred to the classical books [11].

Historical note



O. Zienkiewicz (1921–2009)

The FE method was developed in the 1960s by, among others, the Greek John Argyris (1913–2004) at the University of Stuttgart, the American Ray William Clough (1920–2016) at the University of California (Berkeley) and the Anglo-Polish Olgierd Zienkiewicz (1921–2009) at the University of Swansea. The main contribution of the latter was to recognize the general potential of FE to resolve problems in areas outside solid mechanics. Signature taken from www.nap.edu.

4.1 Outline of the finite element method

As mentioned, FE is probably the most advanced method for the solution of multi-coupled problems, however, for these applications the method involves complex mathematical concepts. Consider the continuum system shown in Figure 9; the FE method is constructed from the following steps:

- i) The continuum domain Ω is divided into subdomains or finite elements Ω_e , interconnected at the nodal points.
- ii) The nodal values of the degrees of freedom are assumed to be the unknown parameters of the problem.
- iii) A set of functions denominated “shape functions” are chosen to interpolate the solution within each finite element in terms of their nodal values.
- iv) The principle of virtual work is applied to the governing equations to obtain “weakened” forms of the problem.
- v) The solution is calculated by solving a set of linear or non-linear equations.

Basically, the resolution of non-linear transient problems implies three steps:

- a) The time interval is divided into small time increments Δt .
- b) The analytical time derivatives are replaced by discrete forms using, for instance, the Newmark- β scheme.

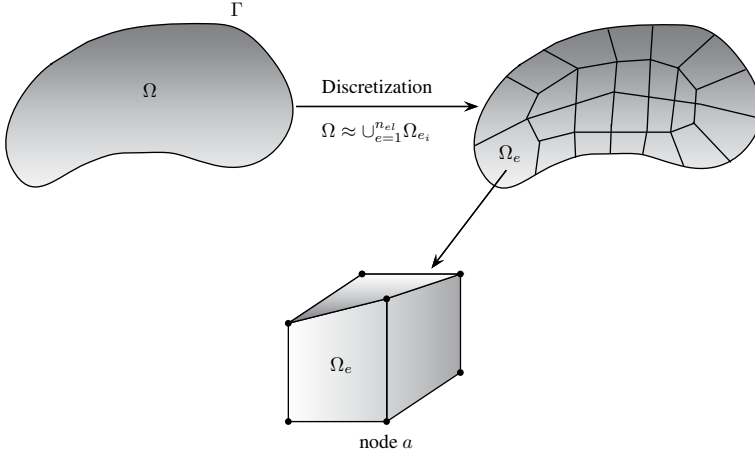


Fig. 9: Finite element discretization of a continuum domain.

- c) The non-linear algebraic problem for each time increment is solved using the Newton–Raphson algorithm.

The assembled non-linear FE equations are written in a residual form \mathcal{R} and are linearized by the derivative:

$$\mathcal{R}_a^k = - \left. \frac{\partial \mathcal{R}_a}{\partial \mathbf{g}_b} \right|^k \mathbf{d}\mathbf{g}_a^k \quad (27)$$

where a, b are the local numbering of two generic nodes, k the Newton–Raphson iteration counter and $\mathbf{d}\mathbf{g}_a^k$ the derivatives of the degrees of freedom at node a . The algorithm for time integration is written as:

$$- \left. \frac{\partial \mathcal{R}_a}{\partial \mathbf{g}_b} \right|^k = c_1 \mathcal{K}_{ab} + c_2 \mathcal{C}_{ab} + c_3 \mathcal{M}_{ab}, \quad (28)$$

where the parameters c_1, c_2 and c_3 are given in [6].

The consistent tangent \mathcal{K} , capacity \mathcal{C} and mass \mathcal{M} matrices are derived for each iteration as:

$$\mathcal{K}_{ab} = - \frac{\partial \mathcal{R}_a}{\partial \mathbf{U}_b}, \quad \mathcal{C}_{ab} = - \frac{\partial \mathcal{R}_a}{\partial \dot{\mathbf{U}}_b}, \quad \mathcal{M}_{ab} = - \frac{\partial \mathcal{R}_a}{\partial \ddot{\mathbf{U}}_b}, \quad (29)$$

where $\mathbf{g}_b^t = \{\mathbf{U}_b, \dot{\mathbf{U}}_b, \ddot{\mathbf{U}}_b\}$ represents the zero, first and second derivatives, respectively. The degrees of freedom at the generic node b are denoted by \mathbf{U}_b .

Finally, the solution is updated using $\mathbf{g}_b^{k+1} = \mathbf{g}_b^k + \mathbf{d}\mathbf{g}_b^k$. Notice that the Newton–Raphson iteration counter should exhibit a quadratic asymptotic rate of convergence if the tangent matrices are correctly calculated.

4.2 Finite element modeling of active materials

The present work deals with a multi-coupled formulation for which each node has five unknowns, namely:

- three mechanical displacements \mathbf{u} in the three Cartesian directions
- voltage potential V
- scalar magnetic potential φ

Consequently, the FE formulation contains a set of five residuals. Notice that the residual for the mechanical displacements is commonly expressed in compact notation by a single equation; however, in matrix notation, it holds three equations due to the fact that \mathbf{u} is a vector.

For the sake of clarity, this section reports the discretizations, residuals and the final assembled FE matrices. For more details on the FE formulation, the reader is referred to [9].

4.2.1 Discretizations

As commented, the continuum domain must be discretized. In this work, this is done by n three-dimensional eight-noded brick elements such that $\Omega \approx \sum_i^n \Omega_e$. Furthermore, standard shape functions \mathcal{N} of Lagrangian type are used to interpolate the unknowns through the element. For simplicity, an isoparametric interpolation is adopted, namely, global coordinates \mathbf{x} and degrees of freedom are approximated by the same \mathcal{N} :

$$\begin{aligned} \mathbf{x} &\approx \mathcal{N}_a \tilde{\mathbf{x}}_a, \\ \mathbf{u} &\approx \mathcal{N}_a \tilde{\mathbf{u}}_a, \quad \dot{\mathbf{u}} \approx \mathcal{N}_a \tilde{\dot{\mathbf{u}}}_a, \\ V &\approx \mathcal{N}_a \tilde{V}_a, \quad \varphi \approx \mathcal{N}_a \tilde{\varphi}_a, \end{aligned} \quad (30)$$

where $\tilde{\mathbf{x}}_a$, $\tilde{\mathbf{u}}_a$, \tilde{V}_a and $\tilde{\varphi}_a$ refer to the nodal value at the local node a , and the Einstein summation convention is applied. Furthermore, (4) and (12) are approximated by:

$$\begin{aligned} \mathbf{S} &\approx \nabla^{\text{sy}} \mathcal{N}_a \tilde{\mathbf{u}}_a = \mathcal{B}_a^{\text{sy}} \tilde{\mathbf{u}}_a, \\ \mathbf{E} &\approx -\nabla \mathcal{N}_a \tilde{V}_a = -\mathcal{B}_a \tilde{V}_a, \\ \mathbf{H} &\approx -\nabla \mathcal{N}_a \tilde{\varphi}_a = -\mathcal{B}_a \tilde{\varphi}_a, \end{aligned} \quad (31)$$

where the derivation operators \mathcal{B} are expressed in matrix notation as:

$$\mathcal{B}_a^{\text{sy}} = \begin{bmatrix} \mathcal{N}_{a,1} & 0 & 0 \\ 0 & \mathcal{N}_{a,2} & 0 \\ 0 & 0 & \mathcal{N}_{a,3} \\ \mathcal{N}_{a,2} & \mathcal{N}_{a,1} & 0 \\ 0 & \mathcal{N}_{a,3} & \mathcal{N}_{a,2} \\ \mathcal{N}_{a,3} & 0 & \mathcal{N}_{a,1} \end{bmatrix}, \quad \mathcal{B}_a = \begin{Bmatrix} \mathcal{N}_{a,1} \\ \mathcal{N}_{a,2} \\ \mathcal{N}_{a,3} \end{Bmatrix}, \quad (32)$$

and $(\cdot,)_i$ denotes differentiation with respect to the i -th Cartesian coordinate.

4.2.2 Residuals

The governing equations reported in Section 3.4 are commonly called strong forms, since they are second-order differential functions of the degrees of freedom \mathbf{u} , V and φ . The term “strong” refers to the higher continuity on the dependent variables. In contrast, the weak forms are often integral expressions that require weaker continuity field variables, namely, they are first-order equations and, consequently, allow an FE discretization. In order to obtain “weakened” forms two procedures exist:

- I. energy principles such as Washizu or Hamilton
- II. weighted residual methods

The first procedure is particularly suited for solid mechanics and structures. On the contrary, the second procedure is more general and can be applied to solve all kinds of partial differential equations. In this sense, the second approach is used in the present work, and it consists of the following steps:

- i) Equilibrium equations (24) are multiplied by arbitrary test functions.
- ii) The divergence theorem is applied to the gradient terms of these equations.
- iii) The Neumann boundary conditions (26) are enforced (the Dirichlet type are automatic).

After the application of the discretizations of (30) and (31) to the weak forms, the three multi-coupled residuals read:

$$\begin{aligned}\mathcal{R}_a^u &= \int_{\Omega_e} \left[\mathbf{B}_a^{\text{SYT}} \mathbf{T}^\top + \mathcal{N}_a(\mathbf{f} - \rho_m \mathcal{N}_b \ddot{\mathbf{u}}_b) \right] d\Omega_e + \oint_{\Gamma_e} \mathcal{N}_a \bar{\mathbf{t}}^{\text{EM}} d\Gamma_e, \\ \mathcal{R}_a^V &= \int_{\Omega_e} \mathbf{B}_a^\top \mathbf{D} d\Omega_e - \oint_{\Gamma_e} \mathcal{N}_a \bar{q}_\Gamma d\Gamma_e, \\ \mathcal{R}_a^\varphi &= \int_{\Omega_e} \mathbf{B}_a^\top \mathbf{B} d\Omega_e.\end{aligned}\quad (33)$$

4.2.3 Assembled matrix

From the residuals of (33) and using (29), the tangent matrices are directly calculated by simple derivations. The final assembled matrix becomes:

$$\begin{bmatrix} \mathcal{K}_{ab}^{uu} + c_3 \mathcal{M}_{ab}^{uu} & \mathcal{K}_{ab}^{uV} & \mathcal{K}_{ab}^{u\varphi} \\ \mathcal{K}_{ab}^{Vu} & \mathcal{K}_{ab}^{VV} & \mathcal{K}_{ab}^{\varphi V} \\ \mathcal{K}_{ab}^{\varphi u} & \mathcal{K}_{ab}^{\varphi V} & \mathcal{K}_{ab}^{\varphi\varphi} \end{bmatrix}^k \begin{Bmatrix} d\ddot{\mathbf{u}}_b^{n+1} \\ d\dot{V}_b^{n+1} \\ d\tilde{\varphi}_b^{n+1} \end{Bmatrix}^k = \begin{Bmatrix} \mathcal{R}_a^u \\ \mathcal{R}_a^V \\ \mathcal{R}_a^\varphi \end{Bmatrix}^k, \quad (34)$$

where the parameter c_3 contains information on the time integration algorithm. As observed, the assembled matrix is a set of five fully coupled equations.

First, no capacity matrices are present, since the current problem is conservative and, consequently, there are no dissipative terms. Second, only the mechanical mass matrices are included, given that the only hyperbolic equation is the linear momentum balance, (7). Third, the main diagonal represents direct (or *passive*) interactions, namely, elasticity, permittivity and permeability, see Table 1. In contrast, the off-diagonal terms are due to the couplings (or *active* interactions) of Table 2. Fourth, the explicit forms of the tangent matrices are reported in [9]. Finally, the set of algebraic equations of (34) is implemented into the research FE code FEAP [12], which belongs to the University of California at Berkeley (USA).

5 Application: Energy production in high-speed railway bridges

This section introduces an overview of high-speed railway bridges with the objective to obtain their main vibration variables. Then, harvesters are numerically simulated by the previous FE formulation, and their energy production is calculated.

5.1 Overview of high-speed railway bridges

Structures have evolved over the years, and this evolution has been driven both by the increasing demands of society and the advances of technology; bridges in general and particularly railway bridges are no exception. Every possibility of reducing traveling times has always been explored with the greatest interest, producing a progressive increase in the speed of these railways. In turn, such increases have led to more demanding requirements for rail infrastructure. Tracks have become heavier and stiffer, a greater radius of curvature has been adopted for bents, cants have also been increased, etc. Like general infrastructure, bridges have to withstand the dynamic effects induced by vehicles traveling at speeds of over 300 [km/h]. Typically, one speaks of high-speed bridges when the design of the line withstands more than 200–250 [km/h].

A wide variety of bridges has been designed to meet the requirements of the new high-speed lines. Because high-speed tracks must avoid sharp curves, long viaducts are very often required to cross over valleys, riverbeds and hollows; additionally, wide streams and estuaries also require long structures. In countries such as Italy, Germany, Spain, USA, China and Japan, prestressed concrete is usually preferred for such long bridges, often (but of course not always) resorting to simply supported, prefabricated decks on top of piers. In China and Japan, a large part of the railway lines are constructed on top of – concrete – viaducts to avoid excessive occupation of land. In addition, this strategy avoids interference between existing and new high-speed lines.

Typical span lengths range from some 30 [m] for simply supported prefabricated decks up to 70 [m] for continuous decks, with some singular constructions featuring more than 150 [m].

Continuous bridges are also present in both steel or mixed construction. Metallic viaducts are typical in France, but some modern designs have also earned a reputation in Spain (spans from 50 [m] to more than 200 [m]). Metallic arches are used in France, China and other countries, with main spans up to some 200 [m]. In Spain, steel arches have also been used in certain singular locations, as is shown in Figure 10 (top), while concrete arches have reached world-record spans in the high-speed lines Madrid-Valencia and Madrid-Portugal. Figures 10 (middle and bottom) and 11 show other representative examples.

In any case, shorter bridges are also required to cross over local roads and small rivers. Simply supported concrete slabs, pseudo-slabs or twin girder bridges are very well suited for such cases, with spans ranging from some 15 up to 40–50 [m]. Twin metallic girder or modern truss bridges are also advisable for single or multiple spans. For shorter spans below some 15 [m], rigid frames are often preferred in order to avoid excessive vibration (Figure 12).

High-speed bridges should to satisfy certain structural requirements in order to guarantee adequate performance. The limits of deflection required for good behavior are rather strict, since passenger comfort is a demanding *serviceability limit state* (SLS) in high-speed transportation. As a rule-of-thumb, in Europe the maximum permitted deflection (or vibration amplitude) under the pass of a high-speed convoy is about $L/2000$, L being the span length. Lower $L/1500$ or higher $L/2500$ values may, of course, be found in practice.

The number of cycles of vibration that the bridge undergoes is variable, depending on the type of train and speed. If resonance or near resonance occurs, vibration will take place during more cycles and with greatest amplitudes. Typically, one cycle of strong oscillation is observed for each bogie when the speed of the train is far from resonance; for a convoy with an axle load pattern such as the one in Figure 13, one would expect around 12 cycles, given that two adjacent bogies are very close in the link between power and passenger cars (also referred to as *coaches*). The motion of the mid-span section would be similar to that shown in Figure 14, in which oscillations of large amplitude arise when the four loads corresponding to the connection between power and passenger cars act at the same time on the bridge ($t = 0.76$ and 5.5 [s]). The approximate maximum amplitudes of the 12 cycles are marked with diamonds in the figure.

Figure 14 corresponds to a simply supported bridge of 22 [m] span, with 5.5 [Hz] of fundamental frequency, a linear mass equal to 22,000 [kg/m] and a 1% damping ratio. The response is computed resorting to the fundamental mode only, which plays a very predominant role in simply supported beams. The total wheelbase of the passenger cars is 18.7 [m], corresponding to a typical Eurostar vehicle. The bogie wheel-



Fig. 10: Top: continuous concrete deck with arch over the motorway Granada–Seville (Spain). Image courtesy of José Lavado Rodríguez (<http://hlestructuras.com>). Middle: double viaduct over the Rhône river in Avignon (France). Image courtesy of Philip Bourret by way of structurae.net. Bottom: simply supported spans on the Madrid-Barcelona high-speed line (Spain) with pre-fabricated concrete beams.



Fig. 11: Archidona (Spain) viaduct: continuous composite twin-girder bridge with upper and lower concrete decks. Image courtesy of Alejandro Castillo Linares (<http://www.acl-estructuras.com>).



Fig. 12: Skewed (left) and straight (right) rigid portal frames. Madrid-Valencia line (Spain).



Fig. 13: Scheme of an articulated train with two power cars and nine passenger cars.

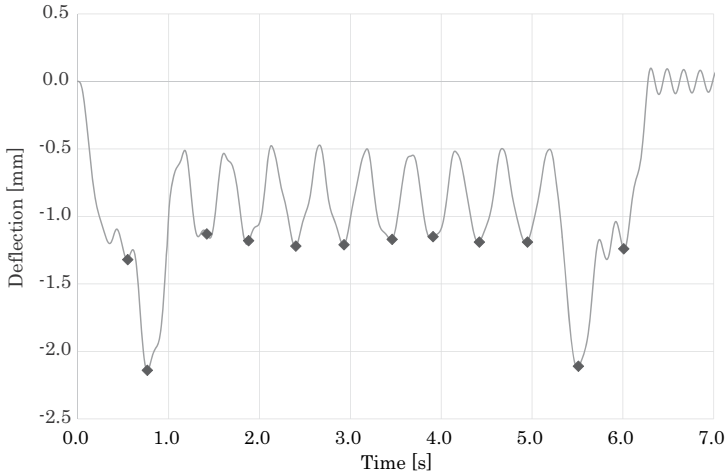


Fig. 14: Typical response in an out-of-resonance situation ($v = 133.2$ [km/h]).

base is 3 [m], with loads per axle of 170 [kN]. A rough number is useful to verify that the analysis yields reasonable results: the static deflection under two point loads concentrated at mid-span, computed solely for the first bending mode is 1.18 [mm]. This is approximately the maximum amplitude of the deflection observed during the passage of the coaches. For the interested reader, the main aspects of the dynamics of railway bridges have been explained well in a number of publications, for instance [7, 13, 14] and [8].

When the vehicle circulates at a speed of resonance (or sub-resonance), more cycles of strong oscillation will appear, because the free vibration induced after the train passage will be larger, and usually the decay of such free vibration is slow; this decay is due to the usual low values of damping of high-speed bridges. Two examples of resonance/sub-resonance are shown in Figures 15 and 16. This resonance occurs when the passage of a coach takes a time lapse equal to one period of the structure; in this example, the vehicle travels at 18.7 [m] in 1/5.5 [s] to reach the first resonance speed. If the time lapse is two, three or more (integer) times the period of the structure, the phenomenon is called sub-resonance (also *resonance of higher order*). Resonance and sub-resonance are jointly referred to simply as *resonances*. In some particular cases, resonances may disappear unexpectedly if the theoretical resonance speed is equal to one of the so-called *cancellation speeds*. This is a particular behavior of simply supported bridges, which is treated in great detail in [7] and [8].

As can be seen, the second resonance is not too strong in this case, and the amplitudes are not much larger in Figure 16 than in Figure 14, except for the free vibration. The reasons beyond maximum or minimum amplitudes of resonances in railway bridges are dealt with in depth in [7]. It should be emphasized that in resonance situations the amplitudes of vibration may be large in general, and the vertical accelera-

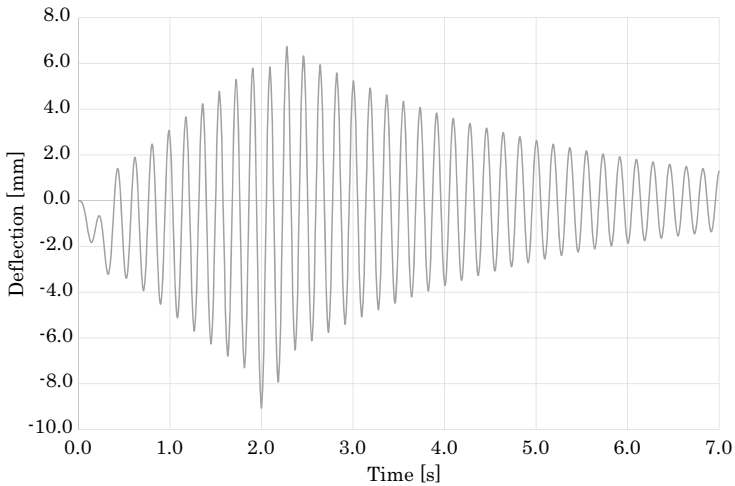


Fig. 15: Typical response in the (first) resonance situation: one oscillation cycle related with the passage of a succession of coaches ($v = 370.3$ [km/h]).

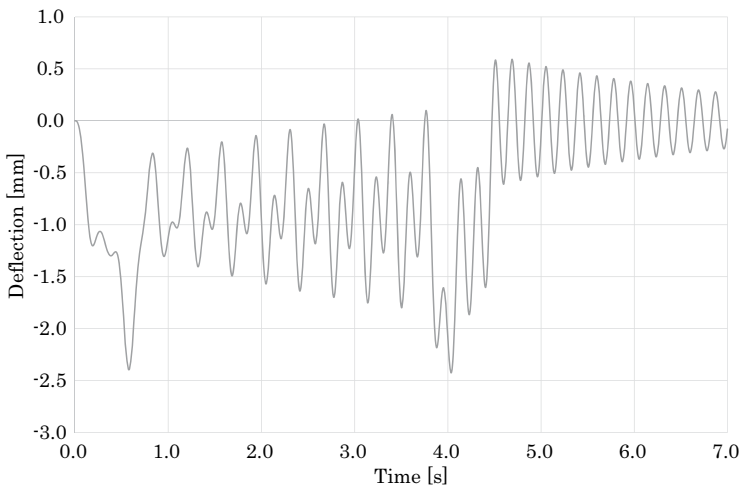


Fig. 16: Typical response in the (second) resonance situation: two cycles of oscillation during the passage of a succession of coaches ($v = 185.15$ [km/h]). This phenomenon is also known as sub-resonance.

tion of the deck could reach unacceptable values. This is also a very demanding SLS for high-speed bridges; usually the vertical acceleration is limited to $0.35 g$ in bridges with ballasted track, while $0.5 g$ is permitted for slab tracks. These limit values are linked to the ballast instability phenomenon and to the loss of the contact phenomenon, respectively; they include an overall security coefficient of 2.0 because of the extreme importance of those phenomena for the running safety, [15].

Other key properties for understanding the dynamic behavior are frequency and damping. Regarding the latter, it should be pointed out that high-speed bridges essentially remain in linear elastic behavior throughout their service life due to their stiffness, vibration and fatigue requirements. Therefore, damping is very low because the structure is virtually undamaged, and values of the critical viscous damping ratio as low as 1% can be expected for prestressed concrete and 0.5% for steel or mixed bridges. These are conservative numbers prescribed by the building codes. It should not be surprising that real values are somewhat higher, a fact that should be duly taken into account for energy harvesting assessments because the vibration levels will be slightly reduced. The reader is referred to, for instance, [13] and [15] for additional information on damping.

As regards the ranges of natural frequencies, a reference is provided in [13]: some values in simply supported bridges would be 10 [Hz] for a 10 [m] span, 6 [Hz] for a 20 [m] span, 4 [Hz] for a 40 [m] span and 2.5 [Hz] for a 70 [m] span; the margins are by no means narrow given the variety of bridge types. The article [16] provides useful ranges for total mass.

The behavior of continuous bridges, frame bridges and arches is more complex than that of the previous cases, due to the greater complexity of their mode shapes and also due to the significant contribution of more modes to the response. The variety of bridge and train types makes it very difficult to give concrete orders of magnitude regarding the vibration amplitudes, frequency levels, etc., particularly in arch bridges due to their singularity. For continuous decks and frames, the limits of deflection are similar (approx. $L/2000$) to the ones with simply supported structures, the frame designs usually being stiffer and, consequently, showing higher frequencies. Even if today's computer codes have very much eased the computational effort, the dynamic analysis of railway bridges is a task that should always be undertaken by expert engineers, especially in the assessment of singular or large structures.

5.2 Numerical modeling of harvesters

A typical vibrating harvester is composed of a substructure, which is typically a metal, an active material (piezoelectric/piezomagnetic) and the proof mass (Figure 17). Due to the mechanical vibration exerted by the passage of a train, the harvester is subjected to mechanical oscillations. As commented, active materials under mechanical causes produce electromagnetic effects that are used to generate power from residual sources. This generation can be used in SHM, a relatively new discipline that uses arrays of sensors/actuators to control the mechanical displacements and to ensure a proper operation of the structure.

Figure 17 shows a sketch of a classic uni-morph harvester, which operates in mode 33; both poling and force directions are the same. As is common, the active material (piezoelectric or piezomagnetic) is bounded by two electrodes, see [17].

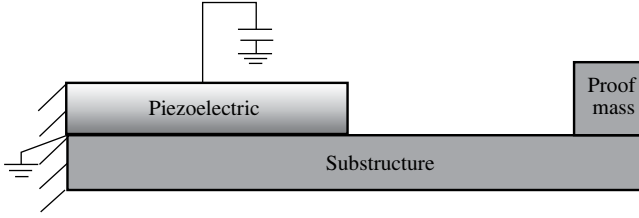


Fig. 17: Sketch of a vibrating harvester composed of piezoelectric/piezomagnetic, substructure and proof mass. Mechanically, it is a cantilever fixed-free beam. Electrically, the electric/magnetic potential is set to zero on the bottom electrode and the top one is connected to a battery.

In the present chapter, this harvester is modeled by the FE formulation described in Section 4. For this purpose, a piezoelectric/piezomagnetic beam of dimensions $30 \times 1 \times 0.5$ [mm] is simulated. Furthermore, the polarization/magnetization is applied along the thickness, and the material properties are taken from [9]:

$$[\mathbf{C}] = \begin{bmatrix} 116 & 77 & 78 & 0 & 0 & 0 \\ & 116 & 78 & 0 & 0 & 0 \\ & & 162 & 0 & 0 & 0 \\ -\text{sym} & & & 89 & 0 & 0 \\ & & & & 86 & 0 \\ & & & & & 86 \end{bmatrix} \times 10^9 \text{ [Pa]} \quad (35)$$

$$[\mathbf{e}^v] = \begin{bmatrix} 0 & 0 & 0 & 0 & 0 & 11.6 \\ & 0 & 0 & 0 & 11.6 & 0 \\ -4.4 & -4.4 & 18.6 & 0 & 0 & 0 \end{bmatrix} \text{ [mPa/V]} \quad (36)$$

$$[\mathbf{e}^\varphi] = \begin{bmatrix} 0 & 0 & 0 & 0 & 0 & 5.5 \\ 0 & 0 & 0 & 0 & 5.5 & 0 \\ 5.8 & 5.8 & 7 & 0 & 0 & 0 \end{bmatrix} \times 10^2 \text{ [mPa/A]} \quad (37)$$

$$[\boldsymbol{\epsilon}] = \begin{bmatrix} 11.2 & 0 & 0 \\ 0 & 11.2 & 0 \\ 0 & 0 & 12.6 \end{bmatrix} \times 10^{-9} \text{ [F/m]} \quad (38)$$

$$[\boldsymbol{\mu}] = \begin{bmatrix} 5 & 0 & 0 \\ 0 & 5 & 0 \\ 0 & 0 & 10 \end{bmatrix} \times 10^{-6} \text{ [H/m]} \quad (39)$$

Numerically, the harvester is meshed by using a structured mesh of 1000 eight-node elements. The mechanical boundary conditions are fixed free to represent the cantilever beam, while both electric and magnetic potentials are set to zero on the bottom electrode, as is shown in Figure 17. Figure 18 shows a three-dimensional view of the FE mesh used for modeling the active material. Notice that the substructure is not represented.

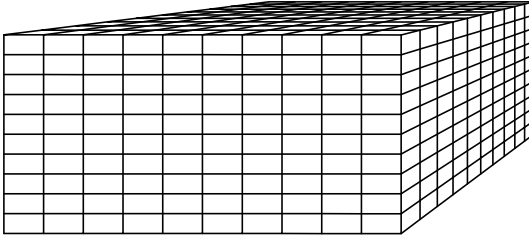


Fig. 18: Perspective view of the FE mesh used for modeling the active material.

The time-history displacement shown in Figure 14 is prescribed in FEAP at the right tip of the beam to obtain the generated electric/magnetic potentials:

- On the one hand, Figure 19 plots the time-history of produced voltage obtained for the harvester made out of piezoelectric material. As observed, the voltage increases with time due to the resonance of the cantilever harvesters and, consequently, the energy produced increases.

Due to this strong increase, the design of resonator harvesters is a challenge for the experimental community. In this sense, the present numerical formulation can be used as a “virtual laboratory”. As observed, a non-negligible potential drop of approximately 12 [mV] is obtained with this simple application. Therefore, the use of several harvesters in a railway bridge produces enough energy to monitor the structure.

- On the other hand, Figure 20 shows the scalar magnetic potentials produced by the piezomagnetic harvester. Again, the cantilever harvester presents resonances for the same mechanical vibrations.

To sum up, it is observed that both piezoelectric/piezomagnetic harvesters show a similar behavior. Nevertheless, the voltage drop is one order of magnitude greater than the magnetic one, monitoring the electric field is easier, and magnetic materials are difficult to miniaturize. In conclusion, the production of energy from mechanical vibration with the former material in high-speed railway bridges looks like the best option.

With regard to the use of the energy production and despite the fact that the potential drop is 12 [mV], this signal could be applied to supply sensors and actuators made out of piezoelectric materials in order to analyze the mechanical displacements of the bridge. As commented, these devices, which produce clean energy, could replace the traditional electro-chemical batteries that pollute the environment. Finally, vibrating harvesters produce alternating current (AC) and, consequently, the use of rectifiers is required. In this sense, the simplest way to rectify the AC is to connect the harvesters with diode junctions, which results in a high efficiency (approximately 84%).

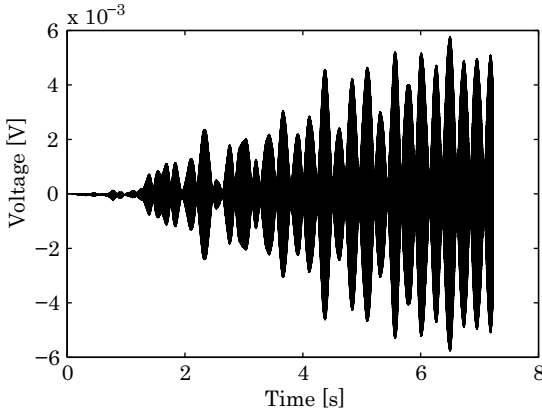


Fig. 19: Produced electric voltage versus time for a piezoelectric harvester.

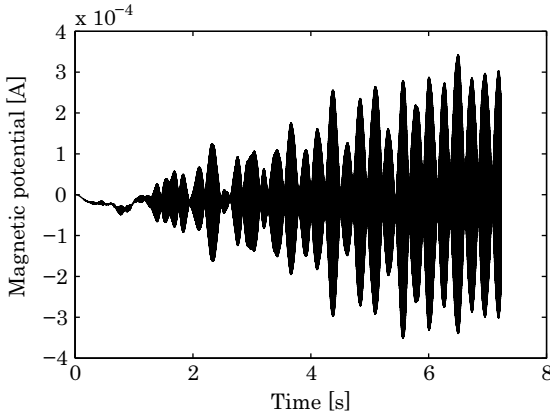


Fig. 20: Produced scalar magnetic potential versus time for a piezomagnetic harvester.

6 Concluding remarks

This chapter has reported a finite element formulation to simulate active materials that couple up to four fields of physics. For the sake of clarity, the chapter outlines the governing equations of several physics branches: continuum mechanics, electrodynamics and thermodynamics. Furthermore, a brief description of the finite element method is also reported.

From a practical point of view, the chapter contains a revision of the main variables and orders of magnitudes of vibrating high-speed railway bridges. For this vibrating application, time-history values are used to obtain the orders of magnitude

of vibrating harvesters. In particular, two cantilever beams made out of piezoelectric and piezomagnetic materials are simulated. Finally, it is concluded that the former are more appropriate for vibrating harvester applications.

In short, this numerical tool allows the design of vibrating harvesters by using a numerical laboratory in contrast to expensive laboratory experiments. For this purpose, this tool could be combined with optimization and probabilistic techniques such as genetic algorithms and Monte Carlo simulation to optimize the harvesters and to perform sensitivity analyses, respectively.

Bibliography

- [1] A. McWilliams. *Smart Materials and Their Applications: Technologies and Global Markets*. BCC Research, 2015.
- [2] J. Hruska. To the stars: After a 25 year hiatus, Nasa restarts plutonium production, 2013. <http://www.extremetech.com/extreme/150756-to-the-stars-after-a-25-year-hiatus-nasa-restarts-plutonium-production>.
- [3] H. S. Kim, J.-H. Kim, and J. Kim. A review of piezoelectric energy harvesting based on vibration. *International Journal of Precision Engineering and Manufacturing*, 12(6):1129–1141, 2011.
- [4] P. Cahill, N. A. N. Nuallain, N. Jackson, A. Mathewson, R. Karoumi, and V. Pakrashi. Energy harvesting from train-induced response in bridges. *J. Bridge Eng.*, 19(9), 2014.
- [5] J. L. Perez-Aparicio, H. Sosa, and R. Palma. Numerical investigations of field-defect interactions in piezoelectric ceramics. *International Journal of Solids and Structures*, 44:4892–4908, 2007.
- [6] R. Palma, J. L. Pérez-Aparicio, and R. L. Taylor. *Non-linear finite element formulation applied to piezoelectric materials with Debye memory*. IEEE/ASME Transactions on Mechatronics, submitted, 2017.
- [7] P. Museros, E. Moliner, and M. D. Martínez-Rodrigo. Free vibrations of simply-supported beam bridges under moving loads: Maximum resonance, cancellation and resonant vertical acceleration. *Journal of Sound and Vibration*, 332:326–345, 2013.
- [8] P. Museros and E. Moliner. *Vibration of simply supported beams under a single moving load: A detailed study of cancellation phenomenon*. International Journal of Mechanical Sciences, in press, 2015.
- [9] J. L. Perez-Aparicio, R. Palma, and R. L. Taylor. Multiphysics and thermodynamic formulations for equilibrium and non-equilibrium interactions: non-linear finite elements applied to multi-coupled active materials. *Archives of Computational Methods in Engineering*, 23(3):535–583, 2016.
- [10] J. L. Jiménez, I. Campos, and M. A. López-Mariño. Maxwell's equations in material media, momentum balance equations and force densities associated with them. *The European Physical Journal Plus*, 128(46):1–6, 2013.
- [11] O. C. Zienkiewicz, R. L. Taylor, and J. Z. Zhu. *The Finite Element Method: The Basis*. Elsevier Butterworth-Heinemann, 2005.
- [12] R. L. Taylor. *FEAP A Finite Element Analysis Program: User Manual*. University of California, Berkeley, 2010.
- [13] L. Frýba. *Dynamics of railway bridges*. Thomas Telford, 1996.
- [14] Y. B. Yang, J. D. Yau, and Y. S. Wu. *Vehicle-bridge interaction dynamics with applications to high-speed railways*. World Scientific Publishing, 2004.

- [15] European Rail Research Institute (ERRI). Ponts-Rails pour vitesses > 200 km/h, 2000. ERRI D-214/RP9.
- [16] A. Doménech, P. Museros, and M. D. Martínez-Rodrigo. Influence of the vehicle model on the prediction of the maximum bending response of simply-supported bridges under high-speed railway traffic. *Engineering Structures*, 72:123–139, 2014.
- [17] F. U. Khan and I. Ahmad. Review of Energy Harvesters Utilizing Bridge Vibrations. *Shock and Vibration*, 2016:21, 2016.

